

## Article

# Enhanced Thermal Stability of Polyphosphate-Dependent Glucomannokinase by Directed Evolution

Heming Sun <sup>†</sup>, Wenlong Zhu <sup>†</sup>, Qinfei Zhang, Ruonan Zheng, Luo Liu <sup>\*ID</sup> and Hui Cao <sup>\*</sup>

Beijing Bioprocess Key Laboratory, Beijing University of Chemical Technology, Beijing 100029, China

<sup>\*</sup> Correspondence: liuluo@mail.buct.edu.cn (L.L.); caohui@mail.buct.edu.cn (H.C.);

Tel.: +86-10-64421335 (L.L.&amp;H.C.); Fax: +86-10-64416428 (L.L.&amp;H.C.)

<sup>†</sup> These authors contributed equally to this work.

**Abstract:** Polyphosphate-dependent glucomannokinase (PPGMK) is able to utilize inorganic polyphosphate to synthesize mannose-6-phosphate (M6P) instead of highly costly ATP. This enzyme was modified and designed by combining error-prone PCR (EP-PCR) and site-directed saturation mutagenesis. Two mutants, H92L/A138V and E119V, were screened out from the random mutation library, and we used site-specific saturation mutations to find the optimal amino acid at each site. Finally, we found the optimal combination mutant, H92K/E119R. The thermal stability of H92K/E119R increased by 5.4 times at 50 °C, and the half-life at 50 °C increased to 243 min. Moreover, the enzyme activity of H92K/E119R increased to 16.6 U/mg, and its enzyme activity is twice that of WT. We analyzed the structure of the mutant using molecular dynamics simulation. We found that the shortening of the hydrogen bond distance and the formation of salt bridges can firmly connect the  $\alpha$ -helix and  $\beta$ -sheet and improve the stability of the PPGMK structure.

**Keywords:** error-prone PCR; directed evolution; site-directed saturation mutagenesis; polyphosphate dependent glucomannokinase



**Citation:** Sun, H.; Zhu, W.; Zhang, Q.; Zheng, R.; Liu, L.; Cao, H. Enhanced Thermal Stability of Polyphosphate-Dependent Glucomannokinase by Directed Evolution. *Catalysts* **2022**, *12*, 1112. <https://doi.org/10.3390/catal12101112>

Academic Editors: Rosa María Oliart-Ros and María Guadalupe Sánchez-Otero

Received: 21 August 2022

Accepted: 22 September 2022

Published: 26 September 2022

**Publisher's Note:** MDPI stays neutral with regard to jurisdictional claims in published maps and institutional affiliations.



**Copyright:** © 2022 by the authors. Licensee MDPI, Basel, Switzerland. This article is an open access article distributed under the terms and conditions of the Creative Commons Attribution (CC BY) license (<https://creativecommons.org/licenses/by/4.0/>).

## 1. Introduction

Mannose-6-phosphate (M6P) participates in a variety of metabolic processes that occur within human cells, such as the synthesis of Golgi and the markers of lysosomal enzymes. M6P can be used for targeted drug delivery in the treatment of cancer [1]. In cell signaling, M6P can specifically bind with mannose-6-phosphate receptors (M6PR), an important signaling receptor in cells. It can be used to treat numerous diseases [2–4]. In recent years, M6P has also received attention in the medical beauty industry for its ability to improve the biomechanical properties of the skin to achieve an anti-aging effect, as well as the treatment of skin redness [5]. However, the chemical synthesis of M6P is inefficient and complicated, and the conversion rate of chemical synthesis of M6P was only 76% [6]. MILTON W. S. has used hexokinase to catalyze the synthesis of M6P, but the substrate is expensive ATP, which greatly increases the cost of industrialization [7]. Our group has used the polyphosphate-dependent glucomannokinase (PPGMK) gene, derived from the *Arthrobacter sp* KM strain, to heterologously express PPGMK. We used  $(\text{NaPO}_3)_6$  to replace ATP to achieve a low-cost, green, and efficient synthesis of M6P [8], with a conversion rate of PPGMK-catalyzed synthesis of M6P close to 100%. However, the half-life of PPGMK is about 40 min at 50 °C. The poor thermal stability of PPGMK does not easily meet the requirements of actual industrial production. This study considers changing the molecular structure of the enzyme to improve the thermal stability of PPGMK. To date, no work has been reported to modify the activity or thermal stability of PPGMK from the *Arthrobacter sp* KM strain. Additionally, the enzymatic activity of PPGMK from diazotrophic *Cyanobacteria* is 2–3 U/mg, and it reaches half-life in about 30 min at 50 °C [9]. A similar enzyme, polyphosphate glucokinase (PPGK), can only catalyze the synthesis

of glucose-6-phosphate (G6P) from glucose, but has no activity on mannose. Zhou et al. simultaneously directed evolution of the enzymatic activity and thermostability of PPGK from *Thermobifida fusca* YX using a petri dishbased double-layer high-throughput screening (HTS) strategy for more efficient production of inositol [10]. Its thermal stability is enhanced by the formation of hydrogen bonds and is related to stabilizing the conformation of the flexible loop. Similarly, the introduction of other chemical bonds, such as disulfide bonds [11], also has a great effect on stabilizing the conformation. Bell et al. rationally designed disulfide bonds to stabilize the conformation of IsPETase [12] and introduced hydrogen bonds to synergistically improve the thermal stability of IsPETase. Enzymes with high thermostability can survive higher reaction temperatures and have a low rate of inactivation. This will improve the efficiency of the catalytic reaction and greatly lower production costs [13,14].

The directional evolution of enzymes is already a well-established technology, including irrational design methods represented by error-prone PCR and semi-rational design and rational design combined with molecular simulation [15,16]. It is more advantageous to use error-prone PCR to create random mutation libraries that make it easier to change the global characteristics of enzymes [17], such as thermal stability [18,19] and pH stability [20]. Moreover, error-prone PCR has also been used to enhance enzyme activity, such as cellulase and chitinase [21,22]. Error-prone PCR in combination with site-directed mutagenesis to further modify the enzyme, which can accumulate benefit mutations, improved mutant performance progressively and effectively [23]. This study employed this particular strategy for the directed evolution of the thermal stability of PPGMK: first, screen out the hot spot amino acids that have an impact on thermal stability in random libraries; second, use the site-directed saturation mutation to choose the most suitable amino acid at this position [24]; finally, obtain the mutant with improved thermostability.

In the process of the directed evolution of proteins, high-throughput methods can greatly improve efficiency [25,26]. The support of high-throughput screening equipment makes a sensitive and efficient detection method essential, such as in the color reaction of H<sub>2</sub>O<sub>2</sub> and horseradish peroxidase (HRP) coupled with ABTS [26]. This method has been used in the screening of mutant libraries [27]. However, it is not used in combination with high-throughput screening equipment, and the efficiency is very low. In this experiment, we coupled this method with glucose oxidase to achieve rapid high-throughput detection of glucose.

PPGMK has catalytic activity on mannose and glucose. There is a special sequence of seven amino acids in the conserved region of glucose/mannose binding area. The mutant lacking the special sequence has no mannose catalytic activity [28]. It is difficult to establish a high-throughput screening method to detect the concentration of mannose or M6P. Glucose can be used as a model substrate for the establishment of a high-throughput screening method. This method of screening with model substrates requires additional validation [26]. Necessarily, the advantageous mutant should be rescreened using mannose as a substrate to demonstrate that it does not affect mannose catalysis.

Molecular dynamics simulation (MD) combines quantum mechanics to analyze the motion trajectories of molecules in a limited framework. MD plays a key role in understanding protein stability and molecular mechanisms, and can also analyze the formation of some chemical bonds. Root mean square deviation (RMSD) represents the relative shift of the entire protein conformation, and a large RMSD value indicates poor stability of the protein; root mean square fluctuation (RMSF) reflects the offset of single amino acid, and a large RMSF value indicates that this amino acid is prone to offset. MD of the enzyme structure can analyze the reasons for the improvement of stability. In addition, we can gain inspiration from MD results, such as predicting various hot spots, and further evolving the thermal stability of the enzyme through semi-rational design methods [29].

## 2. Results

### 2.1. Construction and Screening of Random Mutation Libraries

We constructed a random mutation library using random selections from the mutant library for sequencing, and controlled the mutation rate at about 1–2 bp/kb. High mutation rates caused most mutants to lose catalytic activity. In addition, unfavorable mutations also conceal advantageous mutations, which increases the difficulty of screening. High-throughput screening of 3000 mutants was carried out using the method in 4.4. The screening method was optimized through a pre-experiment. It was found that when the residual glucose concentration was 0–10 mM,  $A_{415\text{nm}}$  was linear with the glucose concentration, the linear relationship is represented as  $y=0.172x + 0.1089$  ( $R^2 = 0.9997$ ), where  $y$  represents  $A_{415\text{nm}}$  and  $x$  represents glucose concentration (mM). When the remaining glucose exceeds 10 mM,  $A_{415\text{nm}}$  is also positively correlated with the glucose concentration, although the linearity is poor. We adjusted the initial concentration and reaction time of the screening reaction so that the residual glucose concentration of WT after the reaction is about 10 mM. The advantageous mutants can be screened more clearly, and  $A_{415\text{nm}}$  can also better reflect the conversion rate of glucose. In addition, it is clearer to use the reciprocal  $1/A_{415\text{nm}}$  of  $A_{415\text{nm}}$  to reflect the quality of the mutant. The larger the value of  $1/A_{415\text{nm}}$ , the more glucose is catalyzed in a certain period of time, and the mutant with the largest value of  $1/A_{415\text{nm}}$  is regarded as the best mutant. We removed the non-mutated and synonymous mutants shown in the sequencing results from advantageous mutants obtained from primary screening, and five mutants were left: G20F, E70V/E119K, K264E, H92L/A138V, and E119V. The calculated positive rate was recorded at 0.167%. We used a 50 mL Erlenmeyer flask to obtain the crude enzymes of each mutant. Then we diluted to the same concentration after purification and performed re-screening with the ABTS method shown in 4.4. The results of re-screening are shown in Figure 1, where it can be seen that H92L/A138V and E119V are better than the wild-type. These two mutants were used as templates for further screening. The SDS-PAGE electropherograms of the wild-type and mutant strains are shown in Figure 2. Both the two enzymes have over-expression bands at 30 kDa.

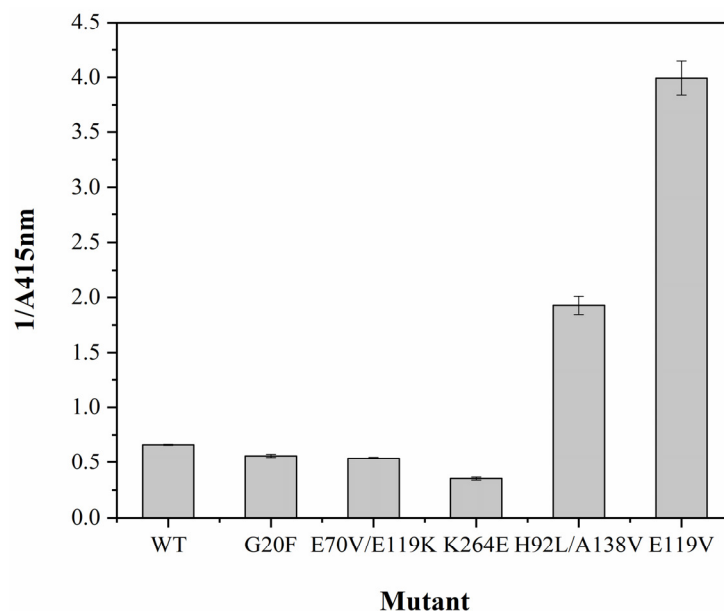


**Figure 1.** The re-screening results of WT, G20F, E70V/E119K, K264E, H92L/A138V, and E119V show that H92L/A138V and E119V are better than the WT (the higher the value of  $1/A_{415\text{nm}}$ , the higher the catalytic efficiency).

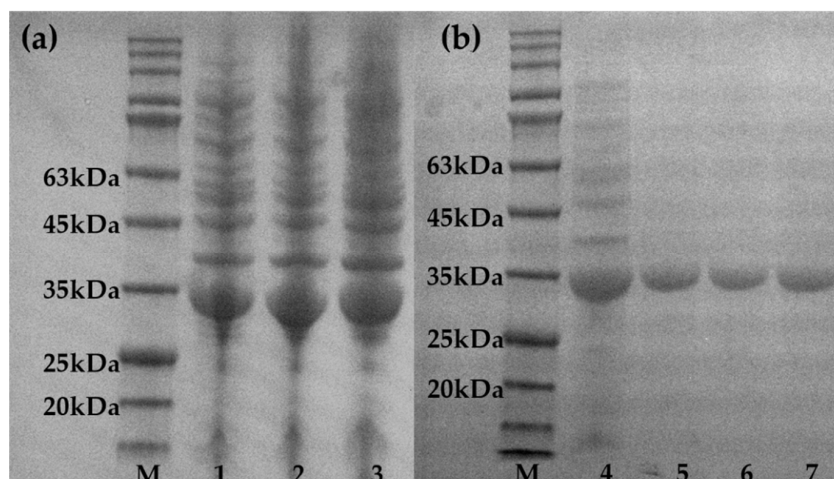


**Figure 2.** (a) SDS-PAGE electrophoresis results of WT, H92L/A138V, and E119V; the mutant has an over-expression band around 30 kDa similar to WT. Lane M: Protein Marker; Lane 1: WT; Lane 2: H92L/A138V; Lane 3: E119V; (b) Comparison of SDS-PAGE electrophoresis results before and after PPGMK purification. Lane M: Protein Marker; Lane 4: WT before purification; Lane 5: WT after purification; Lane 6: H92L/A138V after purification; Lane 7: E119V after purification.

## 2.2. Construction and Screening of Site-Directed Saturation Mutation Libraries

Through random mutation screening we identified three sites that have impacts on thermal stability: H92, E119, and A138, specifically. To further explore which amino acids at these three sites contribute more to the improvement of thermal stability, site-directed saturation mutations were carried out at the three sites, respectively. A site-directed saturation mutant library was constructed by the method of 4.4, and 400 mutants were screened at each site. The advantageous mutants at each point were screened.

After purification with a nickel column, the protein concentration was determined by the Coomassie brilliant blue method and diluted to the same concentration. We used the ABTS method shown in 4.4 for re-screening. When we compared the results with wild-type and H92L/A138V, E119V mutants, we screened out mutants with significantly lower  $A_{415\text{nm}}$  and selected the best mutation. Accordingly, it was determined that the best mutant amino acids at the three positions were H92K, E119R, and A138R. The results of re-screening are shown in Figure 3:

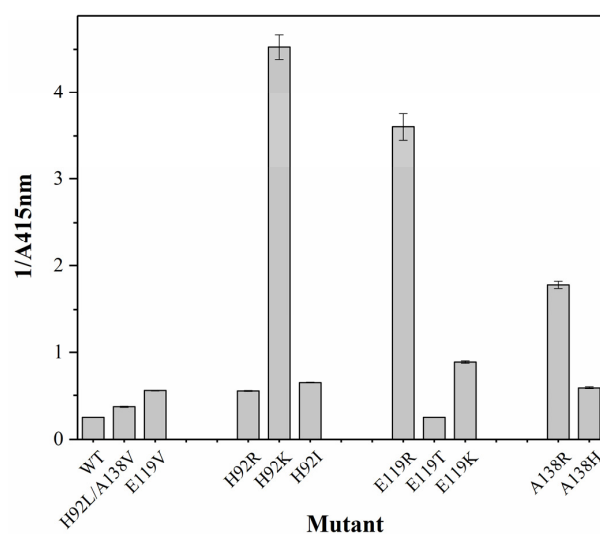


**Figure 3.** The re-screening results of WT, H92L/A138V, E119V, H92R, H92K, H92I, E119R, E119T, E119K, A138R, and A138H show that H92K, E119R, and A138R are the best mutations at the three sites, respectively (the higher the value of  $1/A_{415\text{nm}}$ , the higher the catalytic efficiency).

### 2.3. Combination and Screening of Mutation Sites

We combined the best mutations observed at the three sites into three mutants: H92K/E119R, H92K/A138R, and E119R/A138R. Then, we determined the enzyme activity of two mutants selected by random mutations, three single-point mutants, and three double-point mutants. These test results are shown in Figure 4. A138R did not increase or decrease the enzyme activity significantly. The increase in enzyme activity of the mutant containing A138R was also less than that of the mutant H92K/E119R, the combination of E119R and H92K. Among them, E119R increased the enzyme activity by about two times and was considered to be representative of the most improved thermal stability of the three mutation sites.

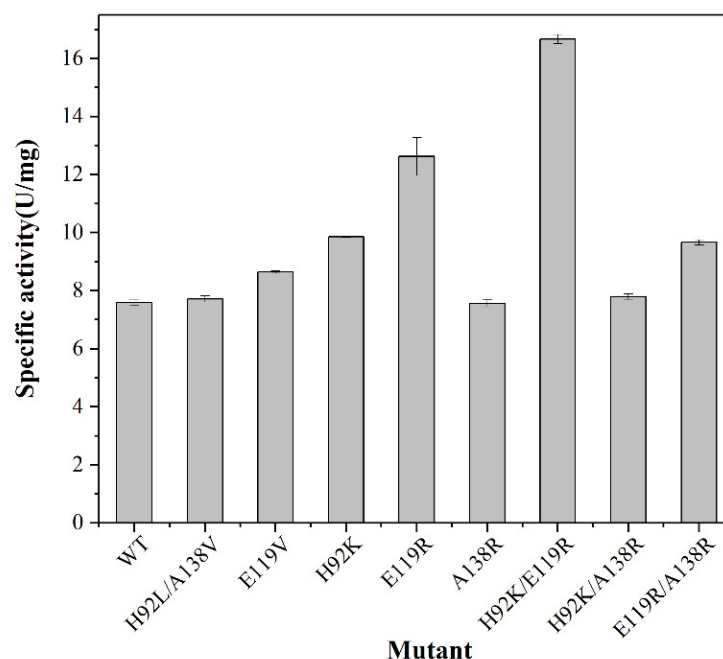


**Figure 4.** Initial enzyme activity test results of WT, H92L/A138V, E119V, H92K, E119R, A138R, H92K/E119R, H92K/A138R, and E119R/A138R at 30 °C (the value of each data point represents the average value).

Next, the half-life of the wild-type and all mutants was determined. The results are shown in Figure 5. The results show that the H92K and E119R mutation sites significantly improve the thermal stability of the enzyme. Connecting the two closest points with the remaining activity of about 50% determines the time when the remaining activity is exactly 50%: the half-life value. The half-life of H92K/E119R at 50 °C can reach 243 min, while that of the wild-type is less than 45 min, and the thermal stability was increased by about 5.4 times. The half-life of H92K was increased by about 1.5 times, and the half-life of E119R was increased by about 2 times. However, the mutants containing A138 did not exhibit high thermal stability or even reduced thermal stability, which resulted in the half-life of H92K/A138R and E119R/A138R being lower than that of the single-point mutant H92K and E119R. Therefore, the three-point combination of the A138R site and the optimal mutant H92K/E119R were not considered.

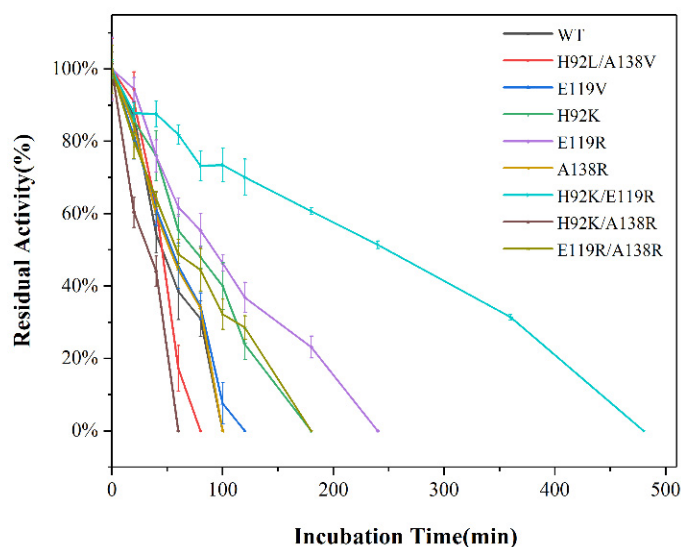


**Figure 5.** Thermal stability of WT, H92L/A138V, E119V, H92K, E119R, A138R, H92K/E119R, H92K/A138R, and E119R/A138R at 50 °C. Heat treatment at 50 °C for 0–480 min, with the reflected enzyme activity of each enzyme without heat treatment recorded at 100%. Determination of the residual vitality, where the value of each data point represents the average value.

#### 2.4. Characteristic Analysis of Mutants

After discarding the mutants A138R, H92K/A138R, and E119R/A138R, the optimal temperature was determined for the remaining mutants and wild-type. At 25–70 °C, the temperature gradient was set to every 5 °C for measurement, and the enzyme activity at the optimal temperature of each enzyme was 100%, calculating the percentage value of enzyme activity of each enzyme. The measurement result is shown in Figure 6. The optimum temperature of WT and H92K was 50 °C, and the optimum temperature of E119 and H92K/E119R increased to 55 °C. It can be seen from Figure 6 that not only does the optimum temperature of E119R and H92K/E119R increase by 5 °C. Moreover, the enzymatic activity decreases more slowly with increasing temperature, while WT and H92K decrease rapidly after the temperature reaches 50 °C.

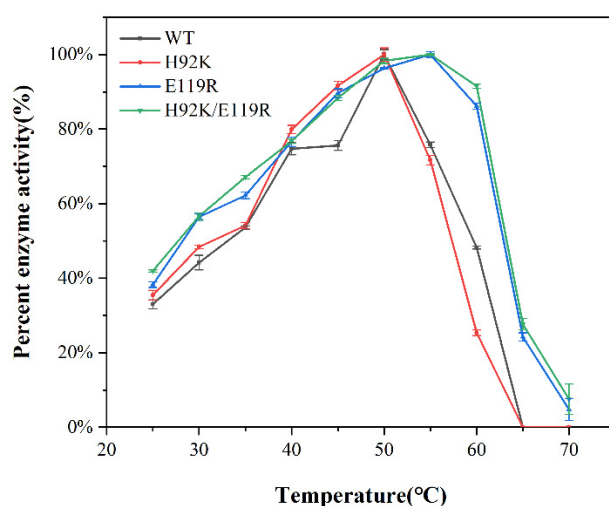


**Figure 6.** The optimal temperature of WT, H92K, E119R, and H92K/E119R was measured, reacted at 25–70 °C for 10 min, and three sets of enzyme activity data were tested every 5 °C. The value of each data point represents the average value.

The kinetic parameters of WT, H92K, E119R, and H92K/E119R on the substrate mannose were tested, including  $K_m$ ,  $V_{max}$ , and  $K_{cat}/K_m$ . The results are shown in Table 1. The

$K_m$  value of WT is 152.5 mM, and the  $K_m$  values of mutants E119R and H92K/E119R are reduced to 24.5 mM and 13.6 mM, and this shows that the E119R mutation site brings better substrate selectivity to PPGMK. Further, H92K has little effect on the  $K_m$  value of the enzyme. The E119R mutation site demonstrated better substrate affinity for mannose, which was also reflected in the H92K/E119R. The  $K_{cat}/K_m$  value of H92K/E119R increased to  $51.5 \text{ s}^{-1} \cdot \text{mM}^{-1}$ , which was much higher than that of the WT, indicating that the H92K/E119R mutant has higher catalytic efficiency.

**Table 1.**  $K_m$ ,  $V_{max}$ , and  $K_{cat}/K_m$  of WT and mutants on mannose.

Mutants	$K_m/\text{mM}$	$V_{max}/\mu\text{mol} \cdot \text{min}^{-1} \cdot \text{mg}^{-1}$	$K_{cat}/K_m/\text{s}^{-1} \cdot \text{mM}^{-1}$
WT	152.5	$5.11 \times 10^3$	8.2
H92K	140.3	$4.55 \times 10^3$	7.9
E119R	24.5	$2.72 \times 10^3$	27.0
H92K/E119R	13.6	$2.86 \times 10^3$	51.5

### 2.5. Structural Analysis of Mutants

To further study the thermodynamic stability before and after the mutation, we used MD to perform 100 ns for wild-type and mutants at 300 K. The MD results are presented in the form of a heatmap in Figure 7, and the values represent the difference values between WT and H92K/E119R. Positive values (red) indicate that the WT has a higher RMSD/RMSF value than H92K/E119R, and negative values (blue) indicate that the WT has a lower RMSD/RMSF value than H92K/E119R.

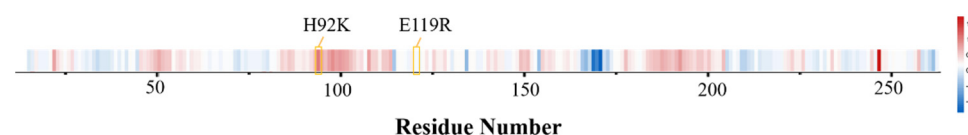


**Figure 7.** The RMSF results of WT and H92K/E119R after MD at 300 K are represented by the difference value, and displayed in the form of a heat map.

According to the heatmap of the RMSF difference values of WT and H92K/E119R at 300 K shown in Figure 7, we can find that, at the mutation site H92K and its surrounding regions, the RMSF value of H92K/E119R was decreased compared with the WT. This shows that the H92K mutation makes the amino acids around H92 more stable, although the improvement in stability is not limited to the H92 single site. Instead, it causes a chain reaction and also improves the stability of nearby amino acids. The decrease in the RMSF of amino acids near the mutation site can also indicate an increase in thermal stability near this position [30]. However, the RMSF of E119R was not significantly reduced, but as a key mutation site, it also slightly improved the stability of nearby amino acids.

The mean RMSD of WT and H92K/E119R at 300 K are  $2.59 \text{ \AA}$ , and  $1.76 \text{ \AA}$ . The mean RMSD after the mutation was reduced by 32%, and as the simulation progressed, the RMSD of the WT rose sharply, whereby it was observed that the RMSD increase of H92K/E119R was much smaller than the WT. This is a strong indication that the thermal stability is improved by the mutation of WT into H92K/E119R.

Running MD at a high temperature, even if using an unreasonable temperature such as 500 K or 600 K [19,31] will only accelerate the unfolding speed of the protein without changing the unfolding path of the protein [32]. To observe the conformational changes of WT and H92K/E119R proteins more intuitively, MD was run at 300 K and 360 K, we superimposed the protein conformations, and compared the results. This result is shown in Figure 8, where the three-dimensional conformation of WT protein at 360 K has a relatively large change compared with that at 300 K. The RMSD is  $3.5140 \text{ \AA}$ , the loop area changes greatly, and the  $\alpha$ -helix and  $\beta$ -sheet parts of the structure collapse seriously. This shows that WT is more sensitive to temperature increases, and its stability is slightly worse. However, we found that the three-dimensional protein conformation of mutant H92K/E119R at 360 K

has little change compared with that at 300 K, and the RMSD is 2.5736 Å. The  $\alpha$ -helix and  $\beta$ -sheet area basically overlap, and only the loop area shows some changes. Before this, the protein structure of PPGMK had been analyzed and the secondary structure had been named [33]. We compared each  $\alpha$ -helix and  $\beta$ -sheet after MD and found that the RMSD of the two  $\alpha$ -helices H6 and H7 of H92K/E119R decreased by more than 50% compared with WT. This indicates that the stability of the two helices improved after mutation. It can be observed that the spatial distance between the two helices and the mutation site is relatively far, which may be due to the mutation affecting the entire protein backbone, resulting in effects on more distant area, whereby a similar situation had also occurred in the directed evolution of cellulases [21]. After running MD at 360 K and 300 K, the RMSD of H92K/E119R was recorded at only 73% of that of the WT. The protein structure of H92K/E119R has a higher degree of coincidence with 300 K after simulation at 360 K than the WT, which further indicates that the thermal stability of H92K/E119R is improved after mutation.

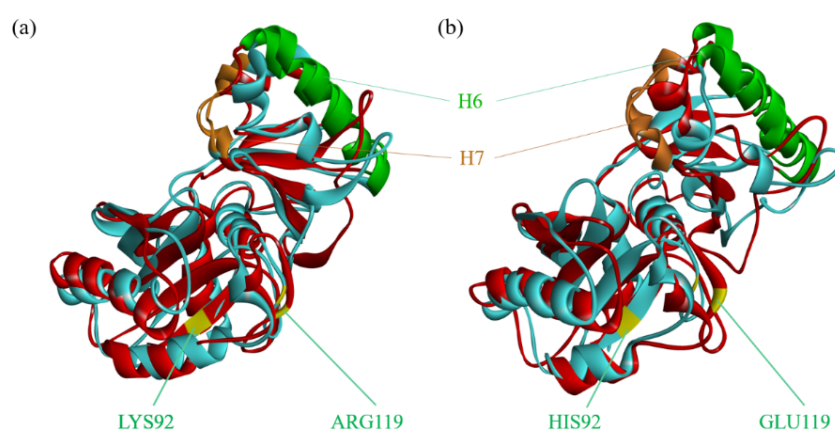


**Figure 8.** Structural comparison of WT and H92K/E119R at different temperatures after 100 ns MD. The area with larger local RMSD is marked. (a) Structural contrast of H92K/E119R at 300 K and 360 K (b) Structural contrast of WT at 300 K and 360 K.

According to the schematic diagram of the protein binding mode shown in Figure 9, it can be seen in H92K/E119R, His-92 changes to Lys-92, which can form a hydrogen bond interaction with Gln-87. Moreover, the hydrogen bond distance is short, with the hydrogen bond length being 3.0 Å, which is less than the 3.5 Å of the traditional hydrogen bond. The shortening of the hydrogen bond distance enhances the bond energy and makes the hydrogen bond more stable. In addition, the carbonyl oxygen of Gln-87 is close to the nitrogen atom of Lys-92, which can form a salt bridge that plays an important role in stabilizing the protein conformation of this part. This may be an important reason for the increase in protein stability. Before the mutation, Glu-119 can form a hydrogen bond with Gln-262, and after the mutation, Arg-119 and Glu-258 form a hydrogen bond interaction, and the hydrogen bond distance is basically the same so that this part of the formation can still remain stable. In addition, after further analysis of the mutation of Glu-119 to Arg-119, we found that the guanidine group of Arg-119 can form a salt bridge with the carboxyl group of Glu-258 after the mutation. This salt bridge can firmly fix the  $\alpha$ -helix and  $\beta$ -sheet. This is of great significance for stabilizing the conformation of the protein [34], and therefore is a key mutation that improves the thermal stability of H92K/E119R.

The combined mutant H92K/E119R is more stable than the H92L/A138V and E119V mutants before the saturation mutation. Leu-92, Val-119, and Val-138 before the saturation mutation are all mutated into aliphatic amino acids, which stabilize the protein by enhancing the hydrophobic force conformation, with no chemical bond changes. After saturation mutation, the thermal stability of the mutant has been significantly improved, which shows that the shortening of the hydrogen bond distance and the formation of salt bridges have significance in improving the stability of the protein conformation. Random mutations

only screen out sites that have a greater contribution to stability, but this position is not necessarily the optimal amino acid.

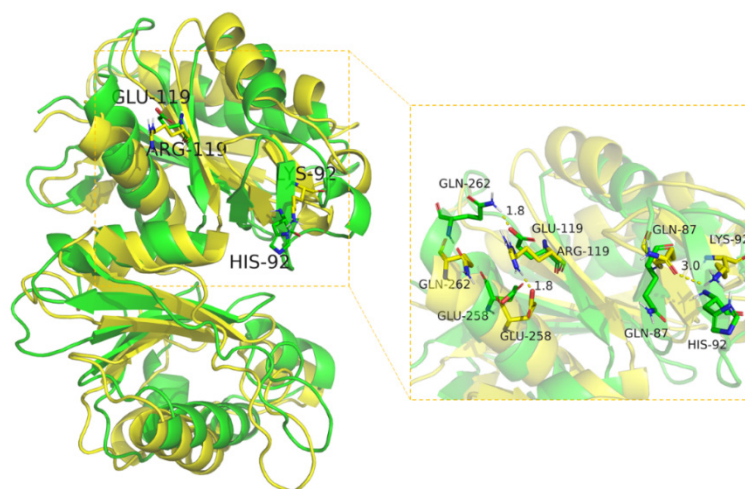


**Figure 9.** The binding mode comparison of WT (green) with H92K/E119R (yellow) protein.

### 3. Discussion

In this study, we heterologously expressed PPGMK in *E. coli*. To improve the thermal stability, an error-prone PCR method was used to construct a random mutation library, where seven amino acid sites were effectively screened from the library. We selected three sites with a significant impact on thermal stability for site-directed saturation mutations. The optimal amino acids at each site were screened out and combined to obtain the optimal mutant H92K/E119R. The half-life of H92K/E119R is 5.4 times than the WT, the optimum temperature is increased by 5 °C, and  $K_{cat}/K_m$  is increased to  $51.5 \text{ s}^{-1} \cdot \text{mM}^{-1}$ . In addition, the catalytic efficiency is greatly improved, and the enzyme activity is increased to two times that of the WT. MD simulations demonstrate that Lys-92 can form hydrogen bonds with Gln-87 at a shorter distance, where the guanidine group of Arg-119 can form a salt bridge with the carboxyl group of Glu-258 to firmly fix the  $\alpha$ -helix and  $\beta$ -sheet. The above data indicate that the mutant H92K/E119R is more suitable for the industrial production of M6P.

When compared with irrational design, the semi-rational design of enzymes allows for a smaller library capacity, smaller screening amounts, and stronger logic. However, the semi-rational design of directed evolution thermal stability is based on the reduction of the B-factor, that is, the reduction of the RMSF value, to determine the amino acid hot spots related to thermal stability, which may not encompass all hot spots. In this experiment, the RMSF at the H92 position was reduced in the H92K/E119R mutant when compared to the WT, but the most critical site of E119 did not show a significant decrease in RMSF. That is to say, the key site E119 could not be found through B-factor screening, and the irrational design simulating natural evolution allowed us to find the E119 site.

At the same time, the irrational design also results in certain shortcomings. About the E70V/E119K mutant initially screened in this experiment, although the most critical site E119 had appeared, it did not show improved thermal stability. This shows that the mutation at the E70 site is not advantageous. Its existence masks the advantageous mutation E119. Moreover, although the mutation E119K has been confirmed as a forward mutation in the rescreening, the effect is not as good as that of E119R. However, rational design is also incomplete.

In conclusion, the combination of irrational design with semi-rational design is undoubtedly a more efficient and precise method for inducing the directed evolution of enzymes with thermostability.

## 4. Materials and Methods

### 4.1. Strains, Plasmid and Reagents

*Escherichia coli* Top10 (used to preserve plasmids) and *E. coli* BL21 (DE3) (used to express the recombinant vector) were purchased from Tiangen Ltd. (Beijing, China). Strains containing the recombinant expression vector pET28a(+) - PPGMK were deposited by our laboratory [8]. Error-prone PCR was performed using the QuickMutation Gene Random Mutation Kit from Beyotime (Shanghai, China). The saturated site-directed mutation was performed using the Mut Express II Fast Mutagenesis Kit V2 kit. Glucose-6-phosphate dehydrogenase (G6PD), mannose-6-phosphate isomerase (MPI), glucose-6-phosphate isomerase (GPI), GOX, and HRP were purchased from Sigma (Shanghai, China), while 2,2'-azino-bis(3-ethylbenzothiazoline-6-sulfonic acid) (ABTS) were purchased from Shanghai yuan ye Bio-Technology Co. Ltd. (Shanghai, China).

### 4.2. Construction of Error-Prone PCR Mutant Library

Extract the plasmid from *E. coli* TOP10, and perform error-prone PCR with the Quick-Mutation TM Gene Random Mutation Kit. The error-prone PCR system was designed with a low mutation rate (0–4.5 bp/kb), whereby the greater the template addition, the lower the mutation rate. Primers used for the error-prone PCR and saturated site-directed mutation are shown in Table 2. Error-prone PCR was performed using primers T7 and T7-Term. PCR was performed for 30 cycles consisting of 3 min at 94 °C, 30 s at 94 °C, 30 s at 55 °C, 1 min at 72 °C, and 10 min at 72 °C.

**Table 2.** PCR primers used for error-prone PCR and saturated site-directed mutation.

Primer	Oligonucleotide Sequence
T7	5'-TAATACGACTCACTATAGGG-3'
T7-Term	5'-GCTAGTTATTGCTCAGCGG-3'
H92-F	5'-CAGCATGGTGTAGTTNNTCTGCAGCTAACGTTGACAAGAGCTGGC-3'
H92-R	5'-CGTTAGCTGCAGAMNNACTACACCATGCTGGATGATGCCTGGGAA-3'
E119-F	5'-TCGTCCAGTTNKGTCATCAACGACGCTGATGCAGCTGGTCT-3'
E119-R	5'-TCGTTGATGACMNNAACTGGACGACCCAGACGTCAGTCAGC-3'
A138-F	5'-ATGGTGCAGGTNNKGGTGTCAAAGGTAAGTACTGTACTGGTCATCAC-3'
A138-R	5'-CCTTTGACACCMNNACCTGCACCATAACGAGCTTCAGCCAGACC-3'
E92K-F	5'-GTAGTTAAGTCTGCAGCTAACGTTGACA-3'
E92K-R	5'-TGCAGACTTAACTACACCATGCTGGATG-3'
E119R-F	5'-CCAGTTCGTGTCATCAACGACGCTGATG-3'
E119R-R	5'-GATGACACGAACTGGACGACCCAGACGT-3'
A138R-F	5'-GCAGGTGCGGGTGTCAAAGGTAAGTACTGTAC-3'
A138R-R	5'-GACACCCCGACCTGCACCATAACGAGC-3'

After the error-prone PCR products were purified, whole plasmid amplification was performed with the Q5 thermo-initiate high-fidelity enzyme. Genes for PPGMK purposes were used as primers. Plasmid pET28a(+) - PPGMK was the template. Error-prone PCR products and large primer PCR products were separately verified by agarose gel electrophoresis. After successful validation, the amplification products were chemically transformed into *E. coli* TOP10, and after amplification and culturing, the plasmid was extracted and transferred into *E. coli* BL21 (DE3), then applied on an LB solid medium with 50 µg/mL Kana for overnight cultivation, where after the mutation rate of the mutant libraries was verified by sequencing.

### 4.3. Construction of Saturated Site-Directed Mutation Library and Combination of the Mutant Sites

We screened out sites that have an impact on thermal stability through error-prone PCR and used Mut Express II Fast Mutagenesis Kit V2 to perform site-directed saturation mutations at these sites. Then we explored whether there were more suitable amino acid mutations. The primers used were H92-F, H92-R, E119-F, E119-R, A138-F, and A138-R. PCR

was performed for 30 cycles consisting of 30 s at 95 °C, 15 s at 95 °C, 15 s at 62 °C, 5 min at 72 °C, and 5 min at 72 °C.

Then, we removed the template with the Dpn I of PCR products and completed the in vitro circularization of linear DNA, which was performed using Exnase II. Mutant libraries were constructed in the same method as 4.2, followed by plasmid extraction and sequencing verification, which determined whether overlapping peaks occur at the mutation site.

We then combined the optimal mutations at each site in pairs. This method is the same as the site-directed saturation mutation of 4.3. The single mutation plasmid in the combination was used as a template. The primers used were E92K-F, E92K-R, E119R-F, E119R-R, A138R-F, and A138R-R, and the combined results were accordingly verified by sequencing.

#### 4.4. High-Throughput Screening

We used the Kbiosystems-K6 Picker to inoculate single colonies into 96 deep well plates. The A1 wells were used as a wild-type control, and each well contained 600  $\mu$ L of LB medium with kanamycin resistance, incubated at 37 °C for 10 h. Then, the 12  $\mu$ L first seed was moved into secondary 96 deep well plates using a high-throughput pipette station, and 600  $\mu$ L 50% of glycerol was added to the first seeds, then stored at  $-20$  °C. Secondary seeds were incubated at 37 °C for 4 h to  $OD_{600nm}$ , reaching 0.6–0.8. An LB medium containing IPTG (the final concentration was 100  $\mu$ g/mL) was added and incubated at 25 °C for 12 h. Following, the precipitation was collected by centrifugation, the precipitation was mixed with 100  $\mu$ L 0.1 M Tris-HCl (pH 8.5). Lastly, all cells were frozen and melted at  $-80$  °C for three times, after which the plate was centrifuged and the supernatant, a crude enzyme, was collected.

A sensitive color-rendering reaction was used for a high-throughput screen, and the schematic diagram is shown in Figure 10. Glucose can be oxidized to gluconic acid and hydrogen peroxide by GOx. Adding a HRP reaction generates free radicals. ABTS appears blue in the presence of free radicals, and it has a linear absorbance with a concentration of 415 nm. GOX competes for all glucose in an extremely short time to terminate the reaction. This method enables the sensitive and rapid detection of the remaining glucose content in the reaction system.

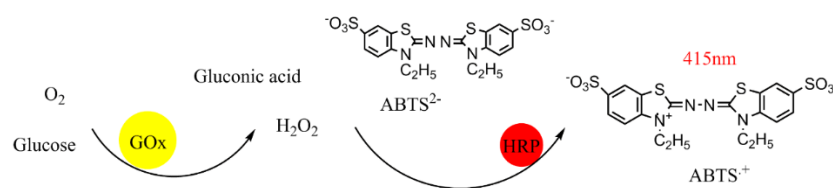


**Figure 10.** Schematic diagram of the color reaction system used in high-throughput screening. Using this method to test  $A_{415nm}$  can quickly detect the remaining concentration of glucose in the system, which can reflect the level of catalytic efficiency of each mutant.

A high-throughput pipette station was used to filter mutants. The reaction system was defined as follows: 30 mM glucose, 30 mM  $(NaPO_3)_6$ , and 10 mM  $MgCl_2$ . The detection system was: GOX 80  $\mu$ g/mL, HRP 20  $\mu$ g/mL, ABTS 7 mg/mL. Next, we added 100  $\mu$ L substrate systems to a 96-well plate, then added 5  $\mu$ L crude enzyme to the 45 °C prewarmed substrate system, observed the 45 °C reaction for 2.5 min, and then added the detection system to terminate the reaction, where after we measured the absorbance with a microplate reader. Controls with lower absorbance than the wild-type were screened in each plate, test-tube cultured and sequenced, and unmutated and synonymous mutants were then finally removed. About 3000 mutants were screened using this method.

The next step was to expand the advantageous mutants, inoculate them from the glycerol tube into 4 mL LB medium (0.1% Kana), culture them at 37 °C for 8 h, and then inoculate 1% of the inoculum into 50 mL LB medium (0.1% Kana), and culture to  $OD_{600nm}$  of

0.6–0.8, add 100 µg/mL IPTG to induce PPGMK expression for 12 h, centrifuge at 8000 rpm to collect bacteria, suspend with 0.1 M Tris-HCl buffer pH 8.5, and ultrasonically disrupt cells to obtain the crude enzyme. The enzyme was purified by affinity chromatography, and the protein concentration was determined by the Coomassie brilliant blue method and verified by SDS-PAGE protein electrophoresis. The enzyme was diluted to the same concentration and rescreened to obtain the advantageous mutant.

#### 4.5. Enzyme Activity Determination

The recombinant vector contained the histidine tag, utilizing the affinity of the histidine tag to nickel ions. The enzyme could use a nickel column for purification, with the purified enzyme being used for enzyme activity assays and kinetic analysis. Buffers containing different concentrations of imidazole (10 mM, 30 mM and 300 mM) were prepared and used as lysis buffer, wash buffer and elution buffer. Use a buffer gradient to remove impurities, and then eluted PPGMK with elution buffer. Replace the buffer with Tris-HCl with a 10kDa ultrafiltration tube. Finally we got pure enzyme. Enzymatic activity assays were performed using two methods. The first was the NADPH method: a 1 mL reaction system was used, including 10 g/L mannose, 10 g/L (NaPO<sub>3</sub>)<sub>6</sub>, 10 mM MgCl<sub>2</sub>, reaction at 30 °C for 10 min, 100 °C boiling water treatment for 3 min to inactivate the enzyme. Add 50 mM NADPNa<sub>2</sub>, 1 U G6PD, 1 U GPI, and 1 U MPI, and then measure the absorption value of NADPHNa<sub>4</sub> at 340 nm. The concentration of NADPHNa<sub>4</sub> is calibrated by measuring the standard curve of NADPHNa<sub>4</sub> and related absorbance. The content of mannose-6-phosphate is determined by the concentration of NADPHNa<sub>4</sub>.

The second method was the HPLC method: The columns were constructed using the American Bole Organic Acid Column Aminex (Hercules, CA, USA) HPX-87H. The flow phase was 5 mM of dilute sulfuric acid, the flow rate was 0.6 mL/min, and the column temperature was 65 °C. The signal was detected with a differential detector, the detection temperature was 40 °C. Mannose peaks at around 9 min. Enzyme activity can only be determined by the detection of substrate reduction.

#### 4.6. Enzymatic Properties

We accordingly tested the optimum temperature of wild-type and mutant types at 25–70 °C and set a temperature gradient every 5 °C. At optimum temperature and pH, we measured the reaction rate of wild-type and mutant strains with 10–100 mM mannose substrate, and set a concentration gradient every 10 mM. The K<sub>m</sub> and V<sub>max</sub> values were calculated using the Lineweaver–Burk method.

The thermal stability of the enzyme was evaluated, because (NaPO<sub>3</sub>)<sub>6</sub> is a protein stabilizer and is often added to food as a food additive, it has a certain protective effect against the enzyme. Therefore, adding the enzyme to (NaPO<sub>3</sub>)<sub>6</sub> for heat treatment instead of Tris-HCl can better reflect the thermal inactivation process of the enzyme in the substrate system. The wild-type and mutant-type were heat-treated in sodium hexametaphosphate for 10 and 240 min, respectively, cooled on ice, added to a substrate of mannose, and reacted at 30 °C for 10 min, the enzyme was treated in boiling water at 100 °C for 3 min to inactivate the enzyme, and then the enzyme activity was measured.

#### 4.7. Structural Analysis

The WT (PDB number: 1WOQ) and its mutant, H92K/E119R, were analyzed using GROMACS 5.1.2. In addition, the 100 ns kinetic simulations were performed at 300 K and 360 K, respectively. Further, the conformation of the last frame at the end of the MD simulation was outputted and we performed a structural superimposed analysis.

## 5. Conclusion

This work improved the thermal stability of PPGMK through directed evolution, solved the problem of easy inactivation of PPGMK during the catalytic production of M6P.

At the same time we improved the enzyme activity of PPGMK, reduces the production cost of M6P, and promotes the process of large-scale and low-cost M6P production.

**Author Contributions:** H.S. and W.Z. performed the experiments. Q.Z. and R.Z. assisted with the simulation calculations. L.L. and H.C. designed the experiment. All authors have read and agreed to the published version of the manuscript.

**Funding:** This work was supported by the National Key Research and Development Program of China (grant number 2021YFF0600703), and the National Key Research and Development Program of China (grant number 2021YFC2101004).

**Data Availability Statement:** Not applicable.

**Conflicts of Interest:** The authors declare no conflict of interest.

## References

1. Mondal, B.; Dutta, T.; Sen Gupta, S. Dual enzyme responsive mannose-6-phosphate based vesicle for controlled lysosomal delivery. *Chem. Commun.* **2021**, *57*, 109–112. [[CrossRef](#)] [[PubMed](#)]
2. Kreiling, J.L.; Montgomery, M.A.; Wheeler, J.R.; Kopanic, J.L.; Connelly, C.M.; Zavorka, M.E.; Allison, J.L.; MacDonald, R.G. Dominant-negative effect of truncated mannose 6-phosphate/insulin-like growth factor II receptor species in cancer. *FEBS J.* **2012**, *279*, 2695–2713. [[CrossRef](#)] [[PubMed](#)]
3. Girsch, J.H.; Jackson, W.; Carpenter, J.E.; Moninger, T.O.; Jarosinski, K.W.; Grose, C. Exocytosis of Progeny Infectious Varicella-Zoster Virus Particles via a Mannose-6-Phosphate Receptor Pathway without Xenophagy following Secondary Envelopment. *J. Virol.* **2020**, *94*, e00800-20. [[CrossRef](#)]
4. Janson, J.; Andersson, G.; Bergquist, L.; Eriksson, M.; Folgering, J.H.A. Impact of chemical modification of sulfamidase on distribution to brain interstitial fluid and to CSF after an intravenous administration in awake, freely-moving rats. *Mol. Genet. Metab. Rep.* **2020**, *22*, 100554. [[CrossRef](#)] [[PubMed](#)]
5. Meunier, M.; Chapuis, E.; Lapierre, L.; Auriol, P.; Paulus, C.; Elbaum, B.; Simoni, E.D.; Sandre, J.; Auriol, D.; Scandolera, A.; et al. Mannose-6-phosphate complex and improvement in biomechanical properties of the skin. *J. Cosmet. Dermatol.* **2021**, *20*, 1598–1610. [[CrossRef](#)]
6. Khanjin, N.A.; Montero, J.L. Synthesis of mannose-6-phosphate analogs: Large-scale preparation of isosteric mannose-6-phosphonate via cyclic sulfate precursor. *Tetrahedron Lett.* **2002**, *43*, 4017–4020. [[CrossRef](#)]
7. Slein, M.W. [20] Synthesis of mannose-6-phosphate by hexokinase. *Methods Enzymol.* **1957**, *3*, 154–157.
8. Zhu, W.L.; Gao, M.M.; Chen, B.Q.; Tan, T.W.; Cao, H.; Liu, L. The Synthesis of Mannose-6-Phosphate Using Polyphosphate-Dependent Mannose Kinase. *Catalysts* **2019**, *9*, 250. [[CrossRef](#)]
9. Albi, T.; Serrano, A. Two strictly polyphosphate-dependent gluco (manno) kinases from diazotrophic Cyanobacteria with potential to phosphorylate hexoses from polyphosphates. *Appl. Microbiol. Biotechnol.* **2015**, *99*, 3887–3900. [[CrossRef](#)]
10. Zhou, W.; Huang, R.; Zhu, Z.; Zhang, Y.-H.P.J. Coevolution of both thermostability and activity of polyphosphate glucokinase from *Thermobifida fusca* YX. *Appl. Environ. Microbiol.* **2018**, *84*, e01224-18. [[CrossRef](#)]
11. Bashirova, A.; Pramanik, S.; Volkov, P.; Rozhkova, A.; Nemashkalov, V.; Zorov, I.; Gusakov, A.; Sinitsyn, A.; Schwaneberg, U.; Davari, M.D. Disulfide bond engineering of an endoglucanase from *Penicillium verruculosum* to improve its thermostability. *Int. J. Mol. Sci.* **2019**, *20*, 1602. [[CrossRef](#)] [[PubMed](#)]
12. Bell, E.L.; Smithson, R.; Kilbride, S.; Foster, J.; Hardy, F.J.; Ramachandran, S.; Tedstone, A.A.; Haigh, S.J.; Garforth, A.A.; Day, P.J. Directed evolution of an efficient and thermostable PET depolymerase. *Nat. Catal.* **2022**, *5*, 673–681. [[CrossRef](#)]
13. Xu, Z.; Cen, Y.K.; Zou, S.P.; Xue, Y.P.; Zheng, Y.G. Recent advances in the improvement of enzyme thermostability by structure modification. *Crit. Rev. Biotechnol.* **2020**, *40*, 83–98. [[CrossRef](#)] [[PubMed](#)]
14. Wu, H.; Chen, Q.M.; Zhang, W.L.; Mu, W.M. Overview of strategies for developing high thermostability industrial enzymes: Discovery, mechanism, modification and challenges. *Crit. Rev. Food Sci. Nutr.* **2021**, *1970508*, 1–18. [[CrossRef](#)]
15. Tamaki, F.K. Directed evolution of enzymes. *Emerg. Top. Life Sci.* **2020**, *4*, 119–127. [[CrossRef](#)]
16. Shivange, A.V.; Hoeffken, H.W.; Haefner, S.; Schwaneberg, U. Protein consensus-based surface engineering (ProCoS): A computer-assisted method for directed protein evolution. *Biotechniques* **2016**, *61*, 305–314. [[CrossRef](#)]
17. Nirantar, S.R. Directed Evolution Methods for Enzyme Engineering. *Molecules* **2021**, *26*, 5599. [[CrossRef](#)]
18. Schmidt, A.; Shvetsov, A.; Soboleva, E.; Kil, Y.; Sergeev, V.; Surzhik, M. Thermostability improvement of *Aspergillus awamori* glucoamylase via directed evolution of its gene located on episomal expression vector in *Pichia pastoris* cells. *Protein Eng. Des. Sel.* **2019**, *32*, 251–259. [[CrossRef](#)]
19. Xing, Y.N.; Tan, J.; Wang, Y.H.; Wang, J.Q. Enhancing the thermostability of a mono- and diacylglycerol lipase from *Malassizia globosa* by stabilizing a flexible loop in the catalytic pocket. *Enzym. Microb. Technol.* **2021**, *149*, 109849. [[CrossRef](#)]
20. Xiang, L.; Lu, Y.H.; Wang, H.; Wang, M.X.; Zhang, G.M. Improving the specific activity and pH stability of xylanase XynHBN188A by directed evolution. *Bioresour. Bioprocess.* **2019**, *6*, 25. [[CrossRef](#)]

21. Basit, A.; Tajwar, R.; Sadaf, S.; Zhang, Y.; Akhtar, M.W. Improvement in activity of cellulase Cel12A of *Thermotoga neapolitana* by error prone PCR. *J. Biotechnol.* **2019**, *306*, 118–124. [[CrossRef](#)] [[PubMed](#)]
22. Menghiu, G.; Ostafe, V.; Prodanovic, R.; Fischer, R.; Ostafe, R. A High-Throughput Screening System Based on Fluorescence-Activated Cell Sorting for the Directed Evolution of Chitinase A. *Int. J. Mol. Sci.* **2021**, *22*, 3041. [[CrossRef](#)]
23. Gao, H.F.; Zhu, R.T.; Li, Z.L.; Wang, W.Y.; Liu, Z.D.; Hu, N. Improving the catalytic efficiency and substrate affinity of a novel esterase from marine *Klebsiella aerogenes* by random and site-directed mutation. *World J. Microbiol. Biotechnol.* **2021**, *37*, 106. [[CrossRef](#)]
24. Balaz, A.M.; Stevanovic, J.; Ostafe, R.; Blazic, M.; Durdic, K.I.; Fischer, R.; Prodanovic, R. Semi-rational design of cellobiose dehydrogenase for increased stability in the presence of peroxide. *Mol. Divers.* **2020**, *24*, 593–601. [[CrossRef](#)] [[PubMed](#)]
25. Xiao, H.; Bao, Z.H.; Zhao, H.M. High Throughput Screening and Selection Methods for Directed Enzyme Evolution. *Ind. Eng. Chem. Res.* **2015**, *54*, 4011–4020. [[CrossRef](#)] [[PubMed](#)]
26. Ye, L.D.; Yang, C.C.; Yu, H.W. From molecular engineering to process engineering: Development of high-throughput screening methods in enzyme directed evolution. *Appl. Microbiol. Biotechnol.* **2018**, *102*, 559–567. [[CrossRef](#)] [[PubMed](#)]
27. Sun, L.H.; Petrounia, I.P.; Yagasaki, M.; Bandara, G.; Arnold, F.H. Expression and stabilization of galactose oxidase in *Escherichia coli* by directed evolution. *Protein Eng.* **2001**, *14*, 699–704. [[CrossRef](#)]
28. Mukai, T.; Kawai, S.; Matsukawa, H.; Matuo, Y.; Murata, K. Characterization and molecular cloning of a novel enzyme, inorganic polyphosphate/ATP-glucomannokinase, of *Arthrobacter* sp strain KM. *Appl. Environ. Microbiol.* **2003**, *69*, 3849–3857. [[CrossRef](#)]
29. Paul, R.K.; Nath, V.; Kumar, V. Structure based virtual screening of natural compounds and molecular dynamics simulation: Butirosin as Dipeptidyl peptidase (DPP-IV) inhibitor. *Biocatal. Agric. Biotechnol.* **2021**, *35*, 102042. [[CrossRef](#)]
30. Parra-Cruz, R.; Jager, C.M.; Li Lau, P.; Gomes, R.L.; Pordea, A. Rational Design of Thermostable Carbonic Anhydrase Mutants Using Molecular Dynamics Simulations. *J. Phys. Chem. B* **2018**, *122*, 8526–8536. [[CrossRef](#)]
31. Purmonen, M.; Valjakka, J.; Takkinen, K.; Laitinen, T.; Rouvinen, J. Molecular dynamics studies on the thermostability of family 11 xylanases. *Protein Eng. Des. Sel.* **2007**, *20*, 551–559. [[CrossRef](#)] [[PubMed](#)]
32. Day, R.; Bennion, B.J.; Ham, S.; Daggett, V. Increasing temperature accelerates protein unfolding without changing the pathway of unfolding. *J. Mol. Biol.* **2002**, *322*, 189–203. [[CrossRef](#)]
33. Mukai, T.; Kawai, S.; Mori, S.; Mikami, B.; Murata, K. Crystal structure of bacterial inorganic polyphosphate/ATP-glucomannokinase—Insights into kinase evolution. *J. Biol. Chem.* **2004**, *279*, 50591–50600. [[CrossRef](#)] [[PubMed](#)]
34. Borgo, B.; Havranek, J.J. Automated selection of stabilizing mutations in designed and natural proteins. *Proc. Natl. Acad. Sci. USA* **2012**, *109*, 1494–1499. [[CrossRef](#)]